

Petroleum pitch: Exploring a 50-year structure puzzle with real-space molecular imaging

Pengcheng Chen^a, Jordan N. Metz^b, Anthony S. Mennito^b, Shamel Merchant^b,
Stuart E. Smith^b, Michael Siskin^b, Steven P. Rucker^b, David C. Dankworth^b,
J. Douglas Kushnerick^b, Nan Yao^{a,**}, Yunlong Zhang^{b,*}

^a PRISM Imaging and Analysis Center, Princeton University, 86 Olden St., Princeton, NJ, 08544, USA

^b ExxonMobil Research and Engineering Company, 1545 Route 22 E., Annandale, NJ, 08801, USA

ARTICLE INFO

Article history:

Received 4 November 2019

Received in revised form

10 January 2020

Accepted 19 January 2020

Available online 24 January 2020

ABSTRACT

Petroleum pitch has played a significant role in carbon science as a key abundant resource for polycyclic aromatic hydrocarbons in making various higher value carbon materials. Despite many detailed studies using advanced characterization techniques over 50 years, the exact nature of the molecular structures of petroleum M-50 pitch and their mesophase products remains unclear, due to the molecular diversity and the low solubility of this material. In this study, we applied real-space single molecule imaging non-contact atomic force microscopy to obtain exact structures of individual molecules, and compared the results from other characterization techniques to validate some of the previously hypothesized average structures. We identified a diverse slate of largely catacondensed polycyclic aromatic hydrocarbons with short alkyl chains, such as methyl and methylene groups. Furthermore, both single core and multi-core structures have been observed, in contrast to previous assertions that only one type would be present. The presence of these structures enables a mechanistic rationalization for their formation and allows potential mechanisms for the thermal conversion of pitch into larger bonding networks to be postulated.

© 2020 Elsevier Ltd. All rights reserved.

1. Introduction

Polynuclear aromatic hydrocarbons (PAHs) featuring high molecular weights and low H/C ratios are enriched in heavy oils, vacuum residues, bitumen, and coals [1]. These aromatic molecules become disfavored in today's quest for energy at lower carbon cost, and transforming them into high performance materials has received considerable interest recently [2–5]. Petroleum pitch is a highly complex mixture of PAHs and has been studied extensively as a premium feedstock for electrode or carbon fiber manufacture [6]. Characterizing their molecular structures, however, remains a challenge, and impedes the development of structure-reactivity and structure-performance relationships necessary to achieving their economic potential for new materials [7,8].

One of the most widely studied petroleum pitches is M-50 (M

from Marathon and number 50 denoting its microcarbon residue content), alternatively known as A-240 (A from Ashland and number 240 denoting its softening point in degrees Fahrenheit). The molecular nature of this complex material has been extensively studied by many groups with the advent of advanced characterization techniques [9–16]. In general, two major challenges were encountered in characterizing and studying this material: (i) the low solubility of the PAHs in most organic solvents and (ii) the inherent complexity of the molecular mixtures in petroleum pitch. As a result, many strategies have been designed to overcome these difficult challenges. Two of the most effective approaches have been extensively used in previous works. The first is the *divide-and-conquer* approach of combining structural analysis with chromatographic separation. Gel permeation chromatography (GPC) was used to segregate molecules according to their molecular weights in the pioneering works in the early 1970s by Smith et al. [9], Dickinson [10,12], and Seshadri et al. [11], and later supercritical extraction by Thies et al. [16–23]. In most of these studies, solvation in quinoline is applied initially to remove the insoluble materials for subsequent fractionation [24]. Chemical functionalization has also been studied to increase solubility and facilitate liquid-phase

* Corresponding author.

** Corresponding author.

E-mail addresses: nyao@princeton.edu (N. Yao), yunlong.zhang@exxonmobil.com (Y. Zhang).

fractionation [25]. The second approach is the deduction of average structures of pitch, or its fractions, based on characterization data of elemental composition, molecular weight, and NMR. Especially, the convenient distinction and quantification of aromatic hydrogens or carbons by NMR is crucial because this structural information cannot be unambiguously assigned from the H/C ratios by elemental composition or double bond equivalent (DBEs) derived from mass spectrometry. The principles and assumptions in the foundational works of Brown and Ladner [26] and Hirsch and Altgelt [27] on ^1H NMR were modified and expanded to include ^{13}C NMR and applied to various complex petroleum mixtures including pitch [9,10].

A few average or representative structures proposed for M-50 pitch or its subfractions are shown in Table 1. The main constituents of all these structures are PAHs, with various sizes ranging from smaller PAHs (1–3 rings) to larger PAHs (up to 10–15 rings). Another common feature is the presence of short alkyl side-chains, predominantly methyl (CH_3) groups in most of these studies; occasionally ethyl or propyl groups. Long alkyl side chains are rare in these models, but their presence was also indicated at low abundance [10]. Heteroatoms and metals are generally insignificant according to previous reports.

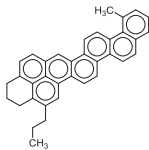
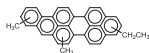
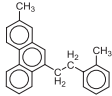
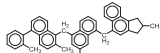
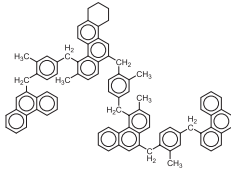
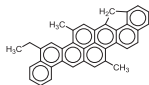
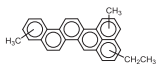
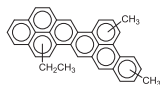
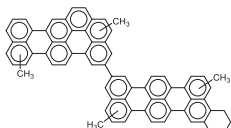
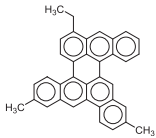
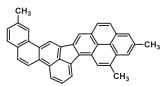
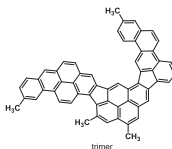
A main difference between these average structures is the presence of linkers between the PAH cores. This discrepancy arises largely from the difficulty for NMR to differentiate internal and bridgehead aromatic carbons for PAH mixtures. Therefore, multiple aromatic cores connected by C_0 (aryl-aryl), C_1 (CH_2), or C_2 (CH_2CH_2) have been proposed by Seshadri et al. [11]. In addition, alicyclic groups (cycloalkanes or naphthenic groups, either five- or six-

membered rings attached to aromatic rings) were also proposed, but only in a few models. The size of PAHs varied over a wide range of fused rings was hypothesized, but the condensation pattern of PAHs was unclear, given the many possible isomers for a specific number of rings. Five-membered rings, either conjugated (such as fluoranthene) or non-conjugated (such as fluorene) were sparsely reported, and was not unambiguously assigned by NMR.

A precise understanding of the structure of pitch was difficult to obtain with the conventional characterization techniques, and proved to be very challenging despite many studies on the same sample even using many different separation and characterization techniques. New insights continue to be obtained by applying advanced analytical tools. For example, a recent study by the Muellen group used high resolution Matrix-Assisted Laser Desorption Ionization – Time of Flight (MALDI-TOF) mass spectrometry combined with ion-mobility separations to shed new light on the carbon number and DBE distribution of large PAHs in pitch [28]. Model compounds such as pyrene- and anthracene-based pitches [29,30] have been used as proxies for natural hydrocarbon mixtures by many groups.

Recently, non-contact atomic force microscopy (nc-AFM) with functionalized CO tips has been applied to characterize small organic PAH compounds (pentacene) [31]. This nc-AFM technique has also been applied to study petroleum samples, including asphaltenes [32], heavy oil mixtures [33], fuel pyrolysis products [34], and marine dissolved organic carbons [35]. In these studies, nc-AFM rendered accessible the structure of heterogeneous mixtures composed of aromatic PAH molecules—even for molecules whose low solubility in organic solvent typically precludes

Table 1
Hypothetical structures proposed for M-50 pitch in previous studies [9,10,12,19].

Entry	Hypothesized overall structure	Hypothesized structures for each fraction		Reference	
1				Dickinson (1980)	
2					Seshadri (1982)
3					Dickinson (1985)
4					Kershaw et al. (1993)
5		 monomer	 dimer	 trimer	Thies et al. (2011)

characterization using traditional techniques. In this paper, we used nc-AFM to identify structures in M-50 pitch and to compare them with previously hypothesized structures. Our results are important for understanding the chemical transformations that occur under high-temperature, and shed light on why this particular pitch is an excellent precursor in forming mesophase pitch and eventually making carbon fiber.

2. Experimental methods

2.1. Thermogravimetric analysis (TGA)

A PerkinElmer Pyris 1 TGA was employed for thermogravimetric analysis. This apparatus can measure mass with a resolution of 0.1 μg . The unit is equipped with a gas manifold to provide high purity dry nitrogen. A standard flow rate of 60 mL/min was utilized. Approximately 10 mg of sample was staged in a platinum pan and the temperature was scanned from 30 to 950 $^{\circ}\text{C}$ at a rate of 3 $^{\circ}\text{C}/\text{min}$ allowing approximately 30 min of nitrogen purge prior to start to establish an inert environment.

2.2. Nuclear magnetic resonance (NMR)

^1H and ^{13}C NMR were obtained with a 400 MHz (100 MHz for ^{13}C) Bruker Ascend Spectrometer with CDCl_3 as the solvent and with 0.003% TMS (tetramethylsilane) as the reference. Data was processed with TopSpin 4.0.6 software.

2.3. Fourier Transform Ion Cyclotron Resonance Mass Spectrometry (FT-ICR MS)

FT-ICR MS was conducted on a Bruker 15T solariX FT-ICR MS (Bruker Daltonics Inc., Billerica, MA, USA). A sample solution in toluene at a concentration of ~ 2000 ppm was prepared and deposited on a MALDI target plate. A Nd YAG laser at 355 nm was employed at $\sim 11\%$ power and around 10 shots to produce molecules in the gas phase and ionize them for introduction to the mass spectrometer. Funnel RF was set at 150 V, and 200 scans were collected from 300 m/z to 2000 m/z in absorption mode and co-added. Data calibration was performed using Bruker Data Analysis 4.5.

2.4. Non-contact atomic force microscopy (nc-AFM)

nc-AFM was carried out with a low-temperature (LT) ultrahigh vacuum (UHV) STM/AFM (CreaTec Fischer & Co., GmbH, Germany) operated under 4.5 K (-268.6 $^{\circ}\text{C}$) and ultrahigh vacuum ($\sim 10^{-11}$ mbar). The sample was deposited from a silicon wafer and flash heated by resistive heating to obtain a low coverage of monolayer molecules on the Cu (111) surface held at 5 K. The temperature of the silicon wafer raised to a few hundred to a thousand degrees within a second as previously described [32–38]. AFM images were obtained with a qPlus sensor and a CO functionalized tip (factor $Q \sim 20000$; stiffness $K \sim 1800$ N/m; resonance frequency 30 kHz). The tip oscillation amplitude was 100 pm.

3. Results

3.1. Physicochemical characterization and thermal analysis

Analysis and characterization of M-50 were conducted to compare with literature data in order to confirm the identity of the M-50 material studied by different groups over the past five decades and batch-to-batch reproducibility (Table 2). Microcarbon

Table 2

Some physicochemical parameters of M-50 petroleum pitch.

Density	1.015 g/mL
Microcarbon residue	51.2 mass%
Element analysis	Mass%
C	92.2
H	5.64
N	0.12
S	0.25
H/C	0.73

residue (MCR, 51.2 wt%), elemental composition and H/C ratio (0.73) show good consistency of this material [9].

Simulated distillation data was obtained to characterize the boiling point profile of the material (Fig. 1a), since the boiling point and volatility are associated with considerations in the sample deposition method in molecular imaging [36]. It shows the b.p. of M-50 starts at 330 $^{\circ}\text{C}$ and that roughly 86.1% of material boils below 750 $^{\circ}\text{C}$. Thermogravimetric analysis (TGA, Fig. 1b) was obtained under nitrogen (N_2) to understand both the volatility and the thermal stability of M-50. It showed that up to 60–70% of weight loss occurred between 300 and 600 $^{\circ}\text{C}$ ($T_{1/2}$ 488 $^{\circ}\text{C}$), which is consistent with simulated distillation and previous data [9]. All the data suggest that the majority of the material is composed of high boiling molecules, without volatile low molecular weight molecules, and the remaining 30–40% are “non-distillable” ultrahigh molecular weight molecules.

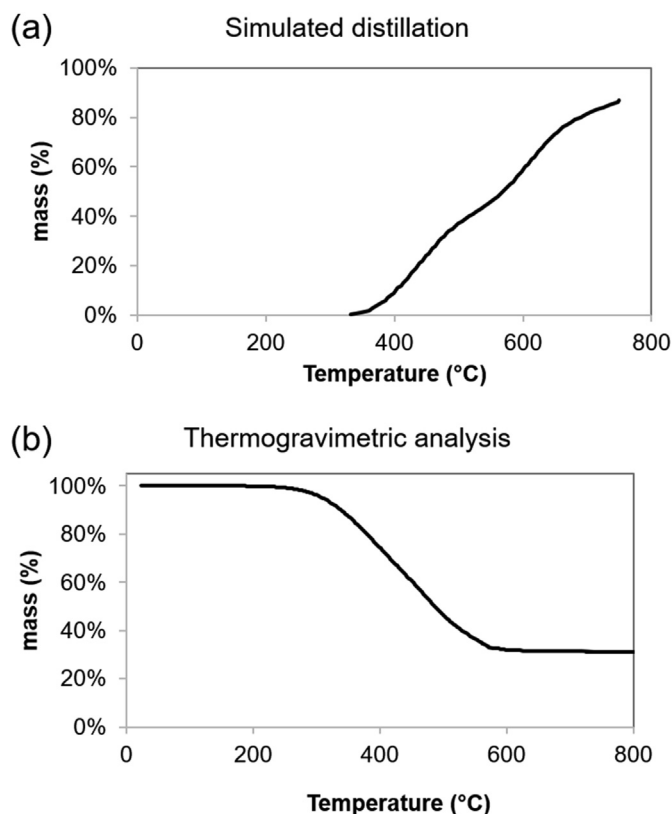


Fig. 1. (a) Simulated distillation and (b) TGA curve of M-50 pitch in nitrogen (N_2) from room temperature up to 800 $^{\circ}\text{C}$.

3.2. NMR spectroscopy and FT-ICR mass spectrometry

Molecular information of M-50, especially the aromatic to aliphatic hydrogen and carbon ratios, can be detected and quantitatively analyzed by NMR spectroscopy. As shown in Fig. 2a, ^1H NMR showed that a significant portion of hydrogens ($\sim 57\%$ mol) in this sample are directly attached to aromatic cores (δ 7–9 ppm). In the aliphatic H region (0–4 ppm), very few are on alkyl groups longer than three carbons; nevertheless they do exist and are observed, as demonstrated by 0.8–0.9 ppm peaks for terminal CH_3 at least 3–4 carbons away from aromatic rings). The side-chains are predominantly short alkyl groups on aromatic rings, such as methyl (2–3 ppm) and ethyl (2 ppm for CH_2). 2D-COSY spectra were obtained to confirm the presence of short chains by the correlation between terminal CH_3 at 0.9 ppm with internal CH_2 at 1.2 ppm, and $\alpha\text{-CH}_2$ at 2.8 ppm (Fig. 2c). ^{13}C NMR confirmed that this sample has predominantly aromatic carbon (δ 100–150 ppm) and few aliphatic carbons (0–30 ppm). The only two groups of peaks detected at 21–22 ppm are consistent with predominantly methyl side chains.

The molecular weight distribution of M-50 was studied with laser desorption FT-ICR MS, and the molecular weight profiles (Fig. 3) are consistent with other ionization method such as field desorption. As shown previously, several humps of peaks are detected with molecules predominantly in the 400–600 and 600–900 Da molecular weight ranges, while minor are <300 or >1100 Da. Although this could be attributed to aggregates of molecules during ionization, it has been characterized as monomers (210–388), dimers (388–645), trimers (645–890), and tetramers (890–1120) by Thies et al. in a series of seminal works on M-50 using MALDI MS [14–16] combined with supercritical extraction [16–23]. Due to the ultrahigh resolution of FT-ICR MS, the molecular formula of all mass peaks can be assigned. Hydrocarbons (HC class) were found to be the predominant species, consistent with very few heteroatoms (S and N) in this sample. The HC classes are mostly composed of PAHs, as shown by the high double bond equivalency ($\text{DBE} = C + 1 - \frac{H}{2} - \frac{X}{2} + \frac{N}{2}$) or Z-classes ($Z = H - 2C$), with the peak around carbon number 40 and Z -56 (DBE 27) and another at carbon number ~ 60 and Z $-82 - -88$. The iso-abundance plot of Z vs. carbon number (Fig. 3b) clearly showed that these PAHs contain around 35–45 and 55–65 carbons.

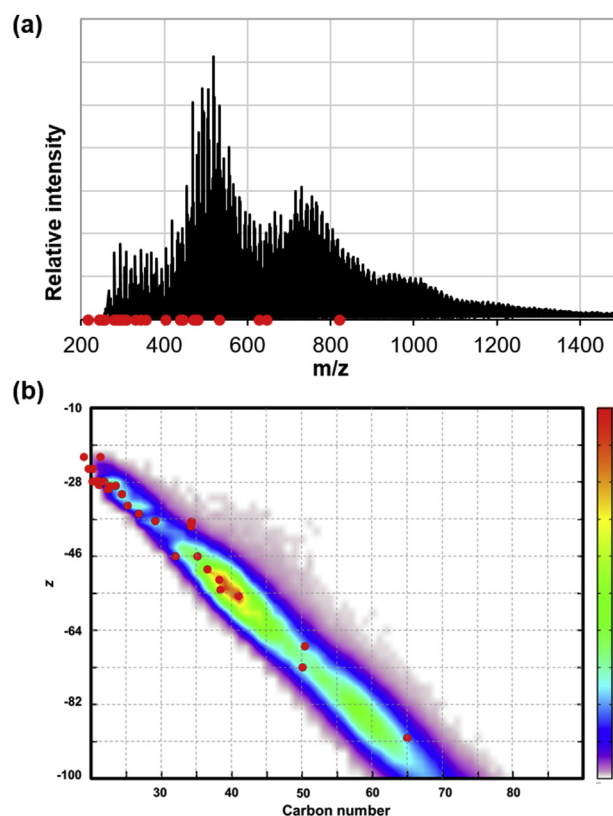


Fig. 3. Mass spectrometry of M-50. (a) laser desorption (LD) ionization FT-ICR MS and (b) the iso-abundance plot of Z-class versus carbon number for hydrocarbon classes, overlaying with molecules observed by AFM imaging (red dots). (A colour version of this figure can be viewed online.)

3.3. Molecular imaging with nc-AFM

The structures in the petroleum M-50 pitch were characterized with a CO-tip AFM similar to previously described [31]. A low coverage of small molecules was prepared and STM imaging (top

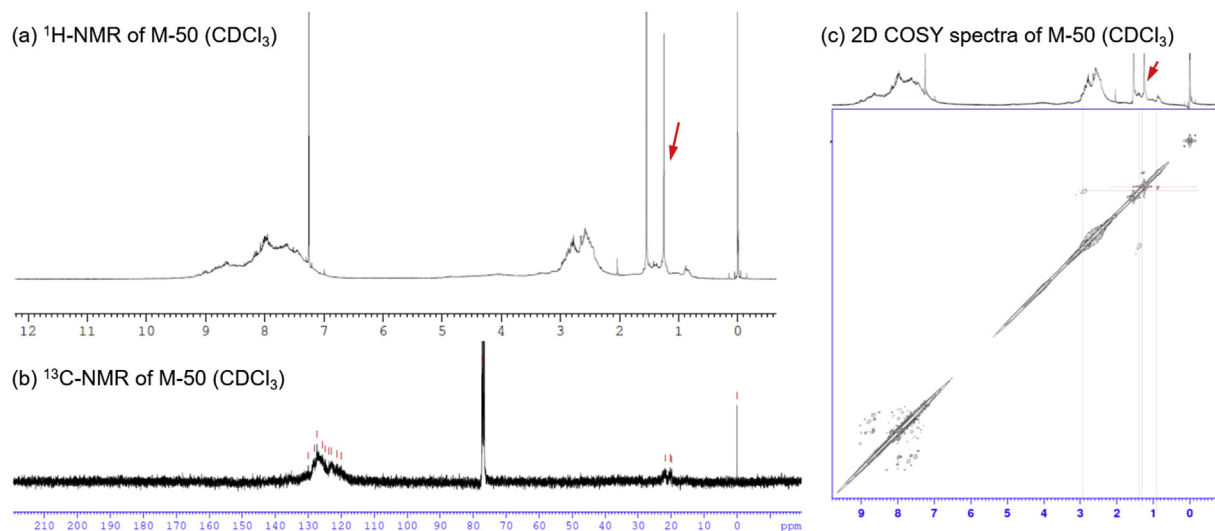


Fig. 2. (a) ^1H NMR spectra of M-50 in CDCl_3 . Solvent residue peaks (indicated as red arrows) include CHCl_3 at δ 7.26 ppm, water at 1.67 ppm, and tetramethylsilane (TMS) at 0 ppm, (b) ^{13}C NMR of M-50 in CDCl_3 . Solvent peak at 77 ppm and (c) 2D COSY spectra for M-50 pitch to show the proton-proton correlations. (A colour version of this figure can be viewed online.)

left panel in Fig. 4) readily confirmed the presence of molecules. But the STM image does not provide detailed chemical structures because STM is a convolution of geometric and electronic effects. Individual molecules were imaged with the CO-functionalized nc-AFM tip to resolve the chemical structures and images are shown in Fig. 4 (also in supporting information). These images took about a month to obtain from several freshly prepared samples. For each sample preparation, an effort was made to image as many molecules as possible in a neighboring area, as most AFM images revealed discernible chemical structures. Some images may seem blurred, despite our attempts to obtain the highest quality images as possible within technical limitations. Some of the causes include thermal drift, conformational flexibility, and mobility of molecules adsorbed on the substrate, etc. Most molecules are around 1.5–2 nm across, with areas of predominantly 2–5 nm². For most molecules, multiple images at different heights, *z*, were taken in order to obtain more detail in specific parts of the structure—especially for molecules with non-planar conformations or *sp*³ carbons. The bright spots in molecular images are caused by the Pauli repulsion of the CO-tip by bulky groups (such as CH₃/CH₂) [31], or nonplanarity of the PAH (aryl-aryl linkage, etc.). The bond-like feature is symptomatic of chemical structure, although recent studies showed that the contrast mechanism is more complicated and new insights have been obtained [39–41].

Structural interpretation of the AFM images (Fig. 4) were made based on visual interpretation of the structure and previous AFM images of known structures, model compounds [37], or of real petroleum samples [33]. Tetrahedral *sp*³ carbons are easily

distinguished from the planar *sp*² carbons, since *sp*³ carbons are 3 dimensional and shown as a protruding feature, and *sp*² carbons are planar in aromatic rings. In addition, chemical principles such as valence structures of PAHs, conformational analysis of nonplanar molecules (aryl-aryl, chair/boat conformation of cyclohexanes) on the surface, and adsorption geometry and their interactions with the substrate are all taken into account [42,43]. An iterative process was conducted for every molecule until the most reasonable structure is reached and assigned (Fig. 5).

Clearly, except for one purely aromatic hydrocarbon molecule (P-26), all remaining molecules have methyl (CH₃) or methylene (CH₂) groups attached to PAHs. While a few molecules have only one methyl group, most have two to three CH₃ or CH₂ or their combinations, with one molecule (P-20) having up to five CH₃/CH₂ groups. There are fewer longer chains but nonetheless they are also observed. For example, ethyl groups are observed in molecules P-6, P-8, P-15, P-21, P-23, P-28, and P-30. Even longer chains were observed in two molecules (P-11, P-14). Naphthenic rings (cycloalkane attached to aromatic rings) are also observed in a few molecules (P-5, P-12). Some of AFM images in Fig. 4 are a challenge to interpret directly, but their assignment is facilitated greatly by our previous work on model compounds [37,44]. A few molecules with two aromatic cores are also observed, such as P-16, P-17, P-21, P-27, and P-28. Assignment of these structures is facilitated by our recent AFM imaging studies using similar model compounds (and unpublished work) [36,37]. This multi-core structure is the hallmark of the average structural model proposed by Seshadri et al. and others [11], but AFM imaged structures clearly showed that

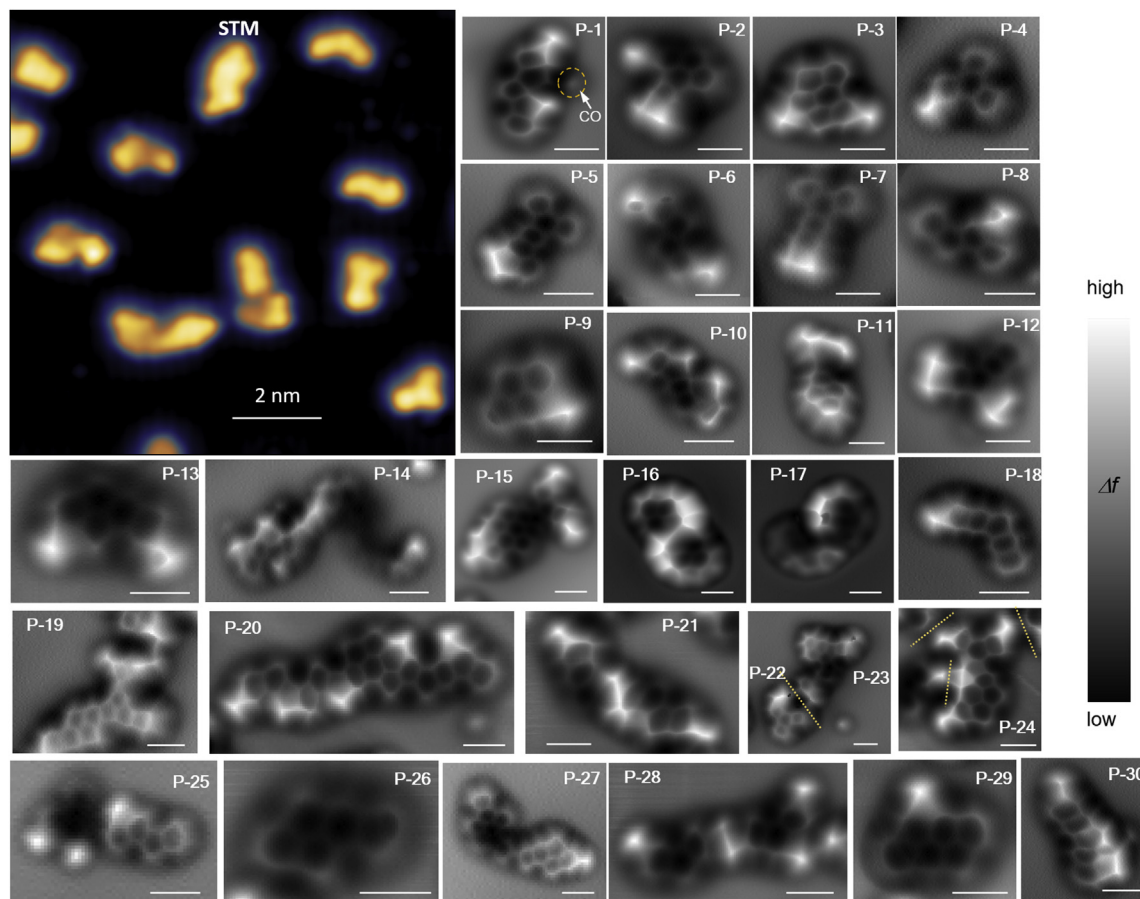


Fig. 4. Images of petroleum pitch M-50 obtained with STM (top left panel) and nc-AFM (P-1 – P-30) using a CO functionalized tip on a Cu (111) surface. STM was collected at 300 mV/200 pA. AFM scale bars are 5 Å and contrast scale is frequency shift Δf (false gradient). (A colour version of this figure can be viewed online.)

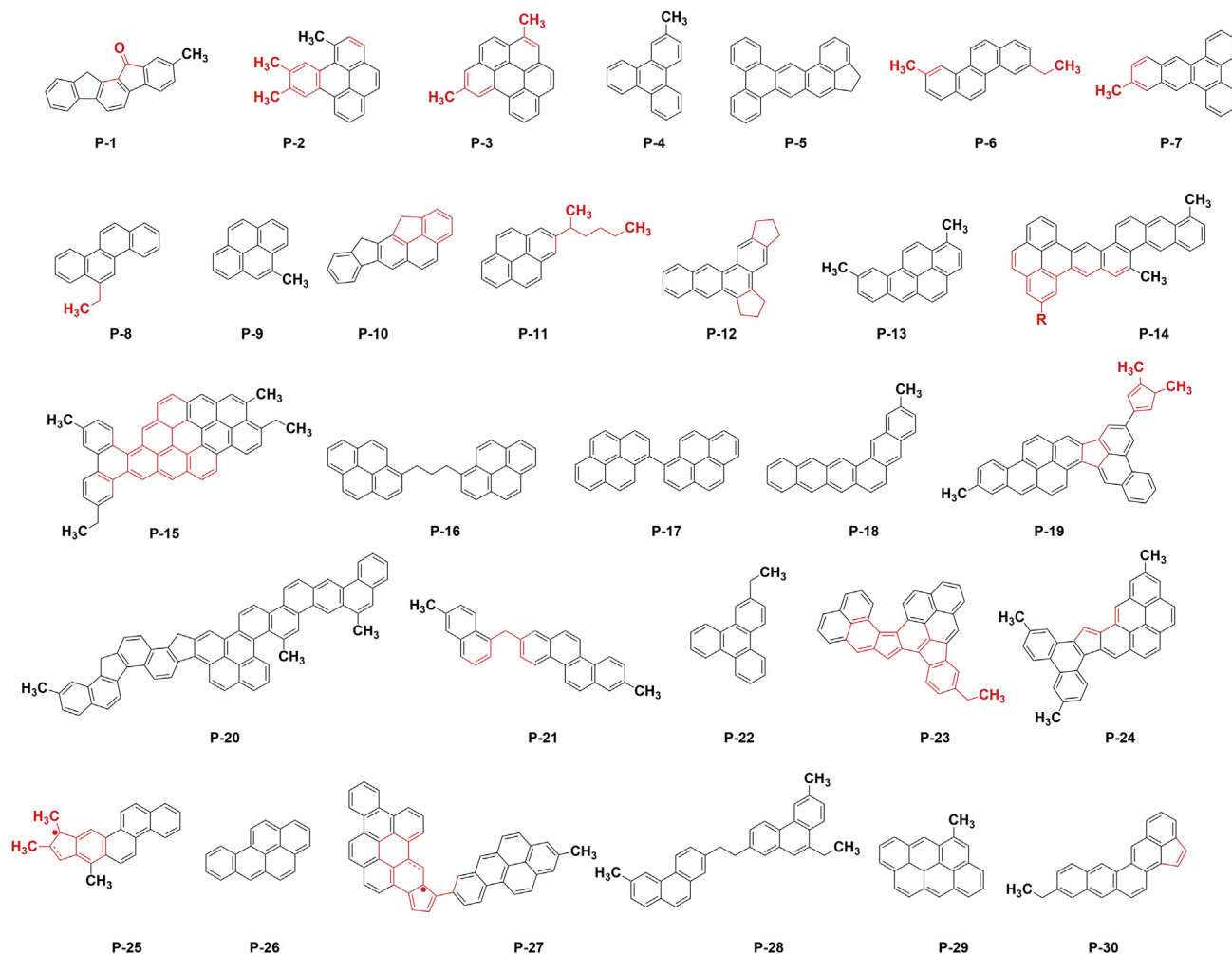


Fig. 5. Chemical structures assigned from the AFM images for M-50 pitch. Regions shown in red indicate uncertain structures. R is any linear or cyclic hydrocarbon moiety which was unassignable. (A colour version of this figure can be viewed online.)

most molecules are inconsistent with this multi-core architecture. Nevertheless it was found in a few molecules, but accounts for only a minority of species at most.

A few molecular images contain a region of dark contrast, often related to a nonalternant hydrocarbon where fully conjugated PAHs are impossible [45], such as P-15, P-25, and P-27. We tentatively assigned them to free radicals with an unpaired electron delocalized across several conjugated aromatic rings, because free radicals tend to have attractive interaction with the CO on the tip through its half-filled molecular orbitals (attractive is dark and repulsive is bright in AFM contrast). Free radicals have previously been observed by AFM in asphaltenes by their singly occupied molecular orbitals (SOMO) [32], or produced by atomic manipulation [37,46]. Free radicals were found a long time ago in petroleum pitch by Singer et al. using Electron Paramagnetic Resonance (EPR) spectroscopy [47,48]. Hence we hypothesize that these free radicals are native species in M-50 pitch which we will study in more detail using EPR in the future.

Finally, we note that although AFM images represent the *exact* structure of individual molecules in pitch (sometimes even with details at the subatomic level), translating these images into conventional skeletal diagrams of chemical structures (e.g., in chicken wire-like structures carbon atoms are implied by vertices of lines representing bonds and hydrogen atoms attached to carbons are

not shown explicitly) without unambiguity is not yet possible. Hence, the uncertain parts in many molecules are highlighted in red in Fig. 5. Recent studies on the contrast mechanism of AFM imaging will help to assign chemical structure to AFM images and overcome this limit [39–41]. Alternatively, machine learning based on AFM images is another promising approach as demonstrated by an initial recent study [49].

4. Discussion

4.1. Many species discovered in M-50 pitch by AFM imaging are new chemical identities

We compared the individual M-50 pitch AFM structures (Fig. 5) with previously hypothesized average structures in the literatures to determine whether they were consistent with the predictions from the ensemble models. Generally, the observed structures were consistent with predictions of PAHs with a few CH_3/CH_2 groups attached, but most of these exact structures are new chemical identities. Significant differences from the hypothesized structures in Table 1 were observed. The diversity of PAH structures is a hallmark of these AFM images. Most of the PAHs found by AFM in M-50 pitch molecules are pyrenes (P-9, P-11, P-16, P-17), benzopyrenes (P-2, P-13, P-26), or benzophenanthrenes (P-4, P-6, P-8, P-

12, P-21, P-22), with very few small PAHs such as naphthalene (P-21) or phenanthrene (P-28), indicating the dominant presence by PAHs with 4–5 rings (13 out of 30 molecules). Very large PAHs with >8 rings were also frequently observed (P-14, P-15, P-19, P-20, P-23, P-24, P-27). Many molecules are catacondensed PAHs (two neighboring rings sharing one side only), and quite a few contain a mixture of cata- and pericondensation; however, few are pericondensed only (two neighboring rings sharing more than one side, e.g. P-3, P-9, P-11, P-16, P-17, P-23, P-29). According to Clar's theory, these few catacondensed PAHs are relatively unstable (P-18, even in P-30). They also obey the *rule of three* (no more than three linear rings in a row) as identified in a recent previous work [50]. Catacondensed or partially catacondensed regions contain reactive sites (e.g., K-regions) which should be important to participate in thermal reactions in forming mesophase. The most stable forms of PAH – such as triphenylene (benzophenanthrene) – are rare but nonetheless also observed (P-4 and P-22) [45,50]. Consistent with previous studies, five-membered rings, either the nonconjugated fluorene type (P-1, P-10, P-20) or the conjugated fluoranthene type (P-19, P-23, P-24, P-27, P-30) are also frequently observed [50]. Thies et al. found that most of the pitch molecules in M-50 are oligomeric in nature based on MALDI MS studies (Table 1) [14–21]. A few AFM structures are consistent with monomers (P-9, P-11) and dimers (P-16, P17) of pyrene species.

4.2. Comparing AFM structures with average structures and NMR data

NMR has been instrumental in obtaining average structures for pitch molecules. It is now possible to validate these NMR-based models with AFM [10]. The ratio of aromatic to aliphatic H and C measured by NMR agrees with that obtained by AFM. The molar fraction of aromatic H atoms in 30 AFM structures was found to be 40–100%, with an average of $69 \pm 15\%$, which is in good agreement with $\sim 57\%$ obtained by ^1H NMR within experimental error (Fig. 2), given that aliphatic moieties in AFM structures can only be underestimated (e.g., R in P-14 is presumed to be H). The molar fraction of aromatic C atoms is 73–100%, with an average $91 \pm 6\%$. The significant short alkyl chains attached to aromatic cores by ^1H and ^{13}C NMR are readily confirmed by the predominance of methyl groups in AFM structures. As noted above, with the exception of two molecule (P-17, P-26) that are unsubstituted aromatic hydrocarbons, almost all molecules have 1–3 methyl groups. The nature of short alkyl chains can now be clarified. In addition to the methyl groups observed in most molecules, various other short alkyl chains are also present, including methylene groups (P-1, P-10, P-20, and likely P-23, P-24, P-25, P-27), ethyl groups (P-6, P-8, P-15, P-22, P-23, P-28, P-30), naphthenic rings (P-12), and aliphatic linkers (P-16, P-21, P-28). The presence of short alkyl chains, especially methyl groups, is a unique feature observed for M-50 in contrast to samples previously studied by AFM imaging [32,33]. For example, coal asphaltenes are composed mostly of PAHs with no substituents [32], while most petroleum samples have a significant portion of aliphatic moieties (R groups) which are hard to characterize with AFM [32,33,45].

These AFM structures are consistent with the early prediction of M-50 pitch by Dickinson et al. [10] that it is composed of highly condensed aromatic ring systems with several short alkyl side chains (average 1.2 carbons per side chain) based on ^1H and ^{13}C NMR analysis. The first hypothesized structure proposed by Dickinson et al. [10] featuring a PAH core comprising up to six fused rings with a methyl, propyl, and an alicyclic ring attached is generally consistent with the AFM structures. Significantly, although not included in the average structure, Dickinson et al. [10] predicted the presence of long aliphatic side chains (carbon

number > 8) at very low concentration based on a sharp peak observed at 1.22 ppm in ^1H NMR spectra (Fig. 2). Indeed, 2D-COSY spectra showed the correlation of the 1.22 ppm peak (middle CH_2 groups which have to be a few carbons away from an aromatic ring) is with a terminal CH_3 at 0.9 ppm. This agrees with one AFM structure observed with a relatively long side chain (P-11), indicating that both techniques are highly sensitive, and providing important cross validation.

Another basic question that remained unclear, or quite controversial in previous studies, is the large-scale architecture of pitch molecules (Table 1), specifically whether PAH cores are fused, or whether they are concatenated with aliphatic linkers. While the structures hypothesized by Dickinson et al. [10,12] and later Kershaw et al. [13] and Thies et al. [14–21] showed predominantly a single PAH core, a dramatically different architecture with multiple (2–3) PAH cores in each molecule connected by multiple methylene (CH_2) or ethylene (CH_2CH_2) linkers was hypothesized by Seshadri et al. [11]. In the study by Dickinson et al. [10], a multicore model was also proposed for another sample (ethylene tar residue) as a comparison with M-50 pitch, indicating the single core structure of M-50 was purposely proposed from careful analysis of NMR data [10]. In addition to the models by Seshadri et al. which are only composed of multiple PAH cores for both M-50 pitch and ethylene pyrolysis tar [11], the MS data (multiple lumps of peaks) that led Thies et al. to hypothesize *oligomeric* (monomer, dimer, and trimer) structures of M-50 also support a multicore structure hypothesis, although only single PAH cores were shown (Table 1) [15]. This controversy on architecture of M-50 pitch is reminiscent of the controversy in the petroleum field on asphaltene structures appearing as archipelagos (multiple PAH cores) or islands (single core, Yen-Mullins model) [1,51–54]. This controversy, which is largely associated with the degree of condensation of PAHs of a given molecular weight, originated from the inability of NMR to accurately quantify the bridgehead vs internal aromatic carbons in a molecule [10–12]. For M-50 pitch, the question can be addressed by the AFM structures shown in Fig. 5, which show both types of structures. While most molecules were shown to be single core architecture, like Dickinson et al. originally proposed [10,12], a few molecules composed of two PAHs are also observed, such as P-16, P-17, P-21, P-28, and perhaps also P-27, similar to the architecture proposed by Seshadri et al. [11], indicating both models need to be considered to describe molecules in M-50 pitch. In addition, the linker between PAH cores, which was an even harder question to address and was proposed as methylene (CH_2) only by Seshadri et al. (Table 1), was shown to be linkers of 0–3 carbon atoms as demonstrated by AFM imaging (Fig. 5). The ability to resolve these structural moieties is facilitated by AFM studies on a few model compounds [37].

4.3. Comparing the average of AFM structures with MS data

Overall, the H/C ratio for AFM structures is 0.71 (Table 3), which agrees well with 0.73 from bulk analysis of this sample. These molecules have 17–65 carbon atoms (average 29) and 12–40 H atoms (average 20), with an average formula of $\text{C}_{29}\text{H}_{20}$. The DBE ranges from 12 to 46 (average 20), or $z - 22 - -90$ (average -38). The molecular weights of 30 AFM structures range from 216 to 821 (average 373). This molecular weight range is consistent with most of previous reports on number average molecular weights of 470–480 [9,10,13] or 380–920 [12] based on vapor pressure osmometry (VPO), or 180–1500 from GPC [11]. Overlaying the molecular weights of the AFM structures with the $\sim 13,500$ mass peaks detected by FT-ICR in the range of 250–1300 is shown in Fig. 3a. This figure shows that while the MW range of 200–820 includes the majority of mass range, most of AFM structures center

Table 3
Calculation and analysis of AFM structures.

Label	Formula	mw	C	H	z	DBE	H/C	% Aromatic H	% Aromatic C
P-1 ^a	C ₂₁ H ₁₄ O	282.3	21	14	-28	15	0.67	64%	90%
P-2	C ₂₃ H ₁₈	294.4	23	18	-28	15	0.78	50%	87%
P-3	C ₂₄ H ₁₆	304.4	24	16	-32	17	0.67	63%	92%
P-4	C ₁₉ H ₁₄	242.3	19	14	-24	13	0.74	79%	95%
P-5	C ₂₈ H ₁₈	354.5	28	18	-38	20	0.64	78%	93%
P-6	C ₂₁ H ₁₈	270.4	21	18	-24	13	0.86	56%	86%
P-7	C ₂₃ H ₁₆	292.4	23	16	-30	16	0.70	81%	96%
P-8	C ₂₀ H ₁₆	256.3	20	16	-24	13	0.80	69%	90%
P-9	C ₁₇ H ₁₂	216.3	17	12	-22	12	0.71	75%	94%
P-10	C ₂₂ H ₁₄	278.4	22	14	-30	16	0.64	71%	91%
P-11	C ₂₂ H ₂₂	286.4	22	22	-22	12	1.00	41%	73%
P-12	C ₂₄ H ₂₀	308.4	24	20	-28	15	0.83	40%	75%
P-13	C ₂₂ H ₁₆	280.4	22	16	-28	15	0.73	63%	91%
P-14 ^b	C ₃₈ H ₂₄	480.6	38	24	-52	27	0.63	75%	95%
P-15	C ₅₁ H ₃₄	646.8	51	34	-68	35	0.67	53%	88%
P-16	C ₃₅ H ₂₄	444.6	35	24	-46	24	0.69	75%	91%
P-17	C ₃₅ H ₁₈	402.5	32	18	-46	24	0.56	100%	100%
P-18	C ₂₇ H ₁₈	342.4	27	18	-36	19	0.67	83%	96%
P-19	C ₄₂ H ₂₈	532.7	42	28	-56	29	0.67	68%	93%
P-20	C ₆₅ H ₄₀	821	65	40	-90	46	0.62	68%	92%
P-21	C ₃₁ H ₂₄	396.5	31	24	-38	20	0.77	67%	90%
P-22	C ₂₀ H ₁₆	256.3	20	16	-24	13	0.80	69%	90%
P-23	C ₂₈ H ₂₂	478.6	38	22	-54	28	0.58	77%	95%
P-24	C ₃₇ H ₂₄	468.6	37	24	-50	26	0.65	63%	92%
P-25	C ₂₄ H ₁₉	307.4	24	19	-29	15.5	0.79	53%	88%
P-26	C ₂₀ H ₁₂	252.3	20	12	-28	15	0.60	100%	100%
P-27	C ₅₀ H ₂₇	627.8	50	27	-73	37.5	0.54	89%	98%
P-28	C ₃₄ H ₃₀	438.6	34	30	-38	20	0.88	50%	82%
P-29	C ₂₃ H ₁₆	292.4	23	16	-30	16	0.70	81%	96%
P-30	C ₂₆ H ₁₈	330.4	26	18	-34	18	0.69	72%	92%
Average	C₂₄H₁₇	372.9 ± 138.0	29 ± 11	20 ± 6	-38.3 ± 16.3	20 ± 8	0.71 ± 0.10	69% ± 15%	91% ± 6%

^a P-1 has one oxygen atom.^b P-14 has an R group which is presumed to be a hydrogen atom in calculations.

on the lower MW end of mass spectrum, especially in the 200–500 range. The isoabundance plot (Fig. 3b) shows that while the majority of AFM structures have < 45 carbon atoms, consistent with MS, a significant fraction of molecules with <30 carbon atoms is inconsistent with sparingly detected ions in this range by FT-ICR MS.

While some discrepancies between the average of AFM imaged structures and FT-ICR MS data should not be surprising since MS measures mass-to-charge ratios (m/z) of ions only and does not detect neutral species, and AFM only measures the frequency-shift due to interactions between the tip and individual species on the Cu(111) surface. The detection of more molecules with a relatively lower molecular weight than MS could be attributed to a bias during the sample preparation of AFM in which a flash heating method is employed. Resistive heating is a well-established method for use with this technique in order to maintain a clean and stable operating condition. In previous studies [36,37,44], we studied a few compounds to understand the effect of flash heating conditions on structures, and we showed that AFM imaging results were relatively consistent with the purity of bulk samples and no cracking observed for compounds of with high boiling points [36]. Other studies on mixtures using nc-AFM also support this result [32–35]. In the current study, random sampling was not strictly executed during AFM imaging of M-50 pitch due to technical and practical limitations, although we didn't pick molecules during imaging. We think random sampling combined with purification or fractionation would be needed in order to obtain quantitative imaging results for diverse samples like M-50 pitch. In addition to this, a few other causes should also be considered: (a) it is unclear if the FT-ICR MS peaks are representative of molecules due to different ionization efficiencies, and (b) larger molecules (hence higher molecular weights) tend to have more complex structures, and

hence are harder to image completely. When they are imaged, the assigned structures based on the resolved moieties will be smaller than the actual structures (e.g., R in #14 is assigned as hydrogen during molecular weight calculation but it is significantly underestimated). Single molecule imaging with nc-AFM does not lend itself to structure determination for large numbers of molecules, but rather to providing exact structures for a limited number of molecules in a mixture. This limitation may be overcome by method advances in the future—such as image analysis by machine learning algorithms [49] or throughput advances in the AFM technique itself, or by chromatographic fractionation of the M-50 pitch, followed by AFM on the individual fractions.

4.4. Proposed mechanism on the formation of AFM structures

Molecular structures should not only be consistent with characterization data, but also with their expected reactivities. Based on the AFM structures and their common patterns observed, the following reaction mechanism for the formation of these observed molecules are proposed. The observed methyl groups, methylene linkages, and five-membered ring with a CH₂ unit in M-50 pitch sample can be rationalized based on the structure of potential petroleum feedstocks and conditions to create them (Fig. 6).

Since M-50 pitch is a heavy fraction (produced from a fluidized catalytic cracking process) which has undergone thermal and catalytic treatment and separation, the native petroleum molecules in virgin crudes may have changed. The substituting alkyl groups on aromatic rings may have undergone β -cleavage, since this is the weakest C–C bond (BDE ~75 kcal/mol) by at least 15 kcal/mol lower than any other bond expected in thermally processed hydrocarbon feeds (typically the aliphatic C–C bond BDE is ~89 kcal/mol) [36]. The primary benzylic free radical after β -cleavage is stabilized by

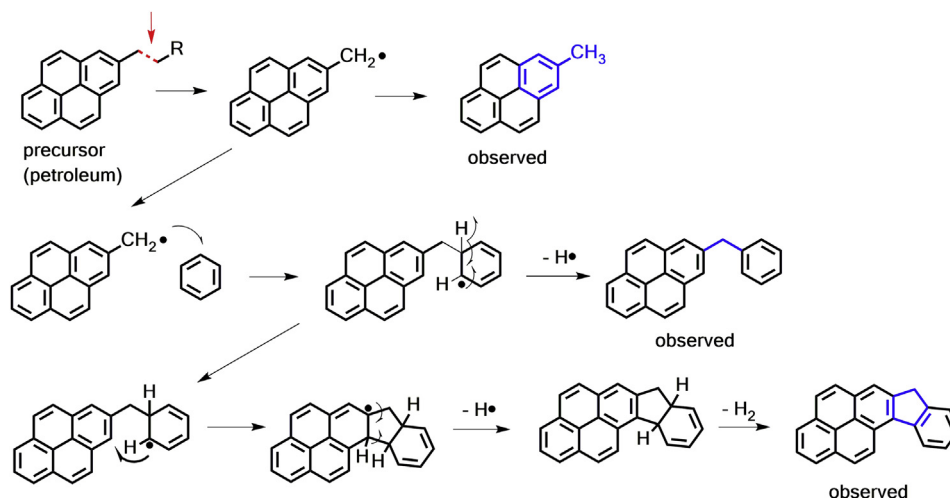


Fig. 6. Proposed radical mechanism on the formation of observed structures from AFM imaging with methyl or methylene substituents or moieties. The substitution position is arbitrary, and the aromatic cores or PAHs are exemplified as benzene and pyrene. The highlighted part in blue indicate the key structural features observed from radical transformation. (A colour version of this figure can be viewed online.)

conjugation to the whole PAH system. The free radical can either abstract a hydrogen atom from another molecule through the chain transfer mechanism to form a terminal methyl group, or attach/alkylate another PAH (especially at sites with enriched double bond character) to produce a molecule with two aromatic cores connected by a CH₂ linker. Thus, a methylene linkage is also expected from such a process, and it is indeed observed in quite a few molecules. However, in most cases, a subsequent ring closure (dehydrocyclization) is facilitated by two neighboring aromatic rings, especially with radicals still present, and hence fluorene-type moieties are formed. This provides an initial rationalization for the formation some major structural features observed in Fig. 5 based on analysis of bond strength. However, this preliminary scheme does not explain all of the structures, and especially the PAH structures. Future studies will address these structures to understand their reactivities under various conditions.

5. Conclusions

The molecular structures in petroleum pitch M-50, an analytical puzzle of five decades' standing, has now been tackled with direct molecular imaging via nc-AFM. The real-space imaging provided structures of molecules to allow for direct comparison with, and validation of, previously hypothesized structures for this material. A diverse range of hydrocarbon molecules, mostly composed of a combination of cata- and pericondensed PAHs with a few short alkyl substituents, has been observed. While methyl (CH₃) groups are prevalent, as previously predicted, other short side chains (e.g., ethyls groups) and five-membered alicyclic rings with one (fluorene) or two methylene (CH₂) groups (naphthenic rings), and even a very few longer alkyl side chains (carbon numbers >5) were observed for the first time. Significantly, the multicore architecture, which was intensely debated, has been confirmed, with linkages varying from zero (directly aryl-aryl linkage) to three aliphatic carbons. The observed AFM structures are consistent with previous data, confirming some features in previously hypothesized average structures, and providing testable hypotheses for new experiments for newly observed features or in discrepancies with previous data. Lastly, the observed AFM structures have been rationalized via their formation mechanism, and the significance of methyl and methylene units in carbon materials pointed out. This work provides numerous opportunities for the recent resurgent interests in

carbon science, such as design of novel model compounds and new experimental tools, or computational models to understand reaction mechanisms of real systems.

Declaration of competing interest

The authors declare that they have no known competing financial interests or personal relationships that could have appeared to influence the work reported in this paper.

CRediT authorship contribution statement

Pengcheng Chen: Methodology, Investigation, Data curation, Writing - review & editing. **Jordan N. Metz:** Data curation. **Anthony S. Mennito:** Data curation. **Shamel Merchant:** Resources. **Stuart E. Smith:** Resources, Writing - review & editing. **Michael Siskin:** Supervision, Writing - review & editing. **Steven P. Rucker:** Project administration, Writing - review & editing. **David C. Dankworth:** Project administration. **J. Douglas Kushnerick:** Project administration. **Nan Yao:** Methodology, Data curation, Funding acquisition, Writing - review & editing. **Yunlong Zhang:** Conceptualization, Investigation, Formal analysis, Writing - original draft, Writing - review & editing.

Acknowledgment

The authors would like to thank Thomas R. Fredriksen for collecting the FT ICR MS data. Y.Z. would like to acknowledge valuable discussions with Dr. Bruno Schuler of Lawrence Berkeley National Laboratory (CA, USA) and Prof. (emeritus) Murray Gray of University of Alberta (Canada). This work was supported by ExxonMobil through its membership in the Princeton E-filliates Partnership of the Andlinger Center for Energy and the Environment. This research made use of Imaging and Analysis Center (IAC) at Princeton University which is supported in part by Princeton Center for Complex Materials, a National Science Foundation (NSF) -MRSEC program (DMR-1420541).

Appendix A. Supplementary data

Supplementary data to this article can be found online at <https://doi.org/10.1016/j.carbon.2020.01.062>.

References

- [1] O.C. Mullins, E.Y. Sheu, A. Hammami, A.G. Marshall, *Asphaltenes, Heavy Oils, and Petroleomics*, Springer Science & Business Media, 2007.
- [2] IEA, *Energy Technology Perspectives 2015*, International Energy Agency, Paris, 2012.
- [3] B.D. Keller, N. Ferralis, J.C. Grossman, Rethinking coal: thin films of solution processed natural carbon nanoparticles for electronic devices, *Nano Lett.* 16 (5) (2016) 2951–2957.
- [4] C. Acuna, R. Marzin, M. De Oteyza, R.C. Perruchoud, Pa Warrendale, *Petroleum Pitch, a Real Alternative to Coal Tar Pitch as Binder Material for Anode Production*, *Light Met.*, 1997, pp. 549–554.
- [5] A.G. Marshall, R.P. Rodgers, *Petroleomics: chemistry of the underworld*, *Proc. Natl. Acad. Sci. U.S.A.* 105 (47) (2008) 18090–18095.
- [6] I. Mochida, *Chemistry of synthesis, structure, preparation and application of aromatic-derived mesophase pitch*, *Carbon* 38 (2000).
- [7] S. Lee, The thermotropic liquid crystalline behavior of mesophase pitches with different chemical structures, *Carbon* 81 (2015).
- [8] E. Frank, L.M. Steudle, D. Ingildeev, J.M. Spörl, M.R. Buchmeiser, Carbon fibers: precursor systems, processing, structure, and properties, *Angew. Chem. Int. Ed.* 53 (21) (2014) 5262–5298.
- [9] W.E. Smith, O.J. Horne Jr., B. Napier Jr., *Characterization and Reproducibility of Petroleum Pitches*, 1974. United States.
- [10] E.M. Dickinson, Structural comparison of petroleum fractions using proton and ¹³C n.m.r. spectroscopy, *Fuel* 59 (5) (1980) 290–294.
- [11] K.S. Seshadri, J.D. Bacha, E.W. Albaugh, Structural characterization of fractions of petroleum pitch and ethylene pyrolysis tar by proton and carbon-13 NMR spectroscopy, *Fuel* 61 (11) (1982) 1095–1100.
- [12] E.M. Dickinson, Average structures of petroleum pitch fractions by proton/carbon-13 NMR spectroscopy, *Fuel* 64 (5) (1985) 704–706.
- [13] J.R. Kershaw, K.J.T. Black, Structural characterization of coal-tar and petroleum pitches, *Energy Fuels* 7 (3) (1993) 420–425.
- [14] W.F. Edwards, L. Jin, M.C. Thies, MALDI-TOF mass spectrometry: obtaining reliable mass spectra for insoluble carbonaceous pitches, *Carbon* 41 (14) (2003) 2761–2768.
- [15] K.W. Hutchenson, J.R. Roebbers, M.C. Thies, Fractionation of petroleum pitch with supercritical toluene, *J. Supercrit. Fluids* 4 (1) (1991) 7–14.
- [16] A. Cristadoro, S.U. Kulkarni, W.A. Burgess, E.G. Cervo, H.J. Raeder, K. Muellen, D.A. Bruce, M.C. Thies, Structural characterization of the oligomeric constituents of petroleum pitches, *Carbon* 47 (10) (2009) 2358–2370.
- [17] W.A. Burgess, J.J. Pittman, R.K. Marcus, M.C. Thies, Structural identification of the monomeric constituents of petroleum pitch, *Energy Fuels* 24 (8) (2010) 4301–4311.
- [18] W.A. Burgess, M.C. Thies, Molecular structures for the oligomeric constituents of petroleum pitch, *Carbon* 49 (2) (2011) 636–651.
- [19] S.U. Kulkarni, H.J. Räder, M.C. Thies, The effects of molecular weight distribution and sample preparation on matrix-assisted laser desorption/ionization time-of-flight mass spectrometric analysis of petroleum macromolecules, *Rapid Commun. Mass Spectrom.* 25 (19) (2011) 2799–2808.
- [20] S.U. Kulkarni, D.F. Esguerra, M.C. Thies, Isolating petroleum pitch oligomers via semi-continuous supercritical extraction, *Energy Fuels* 26 (5) (2012) 2721–2726.
- [21] D.F. Esguerra, W.P. Hoffman, M.C. Thies, Fractionation of an oligomeric pyrene pitch via supercritical extraction, *J. Supercrit. Fluids* 79 (2013) 170–176.
- [22] D.F. Esguerra, W.P. Hoffman, M.C. Thies, Liquid crystallinity in trimer oligomers isolated from petroleum and pyrene pitches, *Carbon* 79 (2014) 265–273.
- [23] M.C. Thies, *Fractionation and Characterization of Carbonaceous Pitch Oligomers: Understanding the Building Blocks for Carbon Materials*, *Polymer Precursor-Derived Carbon*, American Chemical Society, 2014, pp. 85–136.
- [24] L.D.d. Castro, Anisotropy and mesophase formation towards carbon fibre production from coal tar and petroleum pitches : a review, *J. Braz. Chem. Soc.* 17 (2006) 1096–1108.
- [25] R.A. Greinke, I.H. n.m.r. technique for characterization of polymerized petroleum pitches, *Fuel* 63 (10) (1984) 1374–1377.
- [26] J.K. Brown, W.R. Ladner, Hydrogen distribution in coal-like materials by high-resolution nuclear magnetic resonance spectroscopy. II. A comparison with infrared measurement and the conversion to carbon structure, *Fuel* 39 (1960) 87–96.
- [27] E. Hirsch, K.H. Altgelt, Integrated structural analysis. Method for the determination of average structural parameters of petroleum heavy ends, *Anal. Chem.* 42 (12) (1970) 1330–1339.
- [28] W. Zhang, J.T. Andersson, H.J. Raeder, K. Muellen, Molecular characterization of large polycyclic aromatic hydrocarbons in solid petroleum pitch and coal tar pitch by high resolution MALDI ToF MS and insights from ion mobility separation, *Carbon* 95 (2015) 672–680.
- [29] I.C. Lewis, Chemistry of pitch carbonization, *Fuel* 66 (11) (1987) 1527–1531.
- [30] R.A. Greinke, I.C. Lewis, Carbonization of naphthalene and dimethylnaphthalene, *Carbon* 22 (3) (1984) 305–314.
- [31] L. Gross, F. Mohn, N. Moll, P. Liljeroth, G. Meyer, The chemical structure of a molecule resolved by atomic force microscopy, *Science* 325 (2009) 1110–1114.
- [32] B. Schuler, G. Meyer, D. Pena, O.C. Mullins, L. Gross, Unraveling the molecular structures of asphaltenes by atomic force microscopy, *J. Am. Chem. Soc.* 137 (31) (2015) 9870–9876.
- [33] B. Schuler, S. Fatayer, G. Meyer, E. Rogel, M. Moir, Y. Zhang, M.R. Harper, A.E. Pomerantz, K.D. Bake, M. Witt, D. Pena, J.D. Kushnerick, O.C. Mullins, C. Ovalles, F.G.A. van den Berg, L. Gross, Heavy oil based mixtures of different origins and treatments studied by atomic force microscopy, *Energy Fuels* 31 (7) (2017) 6856–6861.
- [34] S. Fatayer, N.B. Poddar, S. Quiroga, F. Schulz, B. Schuler, S.V. Kalpathy, G. Meyer, D. Perez, E. Guitian, D. Pena, M.J. Wornat, L. Gross, Atomic force microscopy identifying fuel pyrolysis products and directing the synthesis of analytical standards, *J. Am. Chem. Soc.* 140 (26) (2018) 8156–8161.
- [35] S. Fatayer, A.I. Coppola, F. Schulz, B.D. Walker, T.A. Broek, G. Meyer, E.R.M. Druffel, M. McCarthy, L. Gross, Direct visualization of individual aromatic compound structures in low molecular weight marine dissolved organic carbon, *Geophys. Res. Lett.* 45 (11) (2018) 5590–5598.
- [36] Y. Zhang, B. Schuler, S. Fatayer, L. Gross, M.R. Harper, J.D. Kushnerick, Understanding the effects of sample preparation on the chemical structures of petroleum imaged with noncontact atomic force microscopy, *Ind. Eng. Chem. Res.* 57 (46) (2018) 15935–15941.
- [37] B. Schuler, Y. Zhang, S. Collazos, S. Fatayer, G. Meyer, D. Perez, E. Guitian, M.R. Harper, J.D. Kushnerick, D. Pena, L. Gross, Characterizing aliphatic moieties in hydrocarbons with atomic force microscopy, *Chem. Sci.* 8 (3) (2017) 2315–2320.
- [38] L. Gross, B. Schuler, N. Pavlicek, S. Fatayer, Z. Majzik, N. Moll, D. Pena, G. Meyer, Atomic force microscopy for molecular structure elucidation, *Angew. Chem. Int. Ed. Engl.* 57 (15) (2018) 3888–3908.
- [39] D. Fan, Y. Sakai, J.R. Chelikowsky, Real-space pseudopotential calculations for simulating noncontact atomic force microscopy images, *J. Vac. Sci. Technol. B* 36 (4) (2018), 04H102.
- [40] P. Hapala, G. Kichin, C. Wagner, F.S. Tautz, R. Temirov, P. Jelinek, Mechanism of high-resolution STM/AFM imaging with functionalized tips, *Phys. Rev. B* 90 (8) (2014), 085421–085429.
- [41] M. Ellner, P. Pou, R. Pérez, Molecular identification, bond order discrimination, and apparent intermolecular features in atomic force microscopy studied with a charge density based method, *ACS Nano* 13 (1) (2019) 786–795.
- [42] F. Huber, J. Berwanger, S. Polesya, S. Mankovsky, H. Ebert, F.J. Giessibl, Chemical Bond Formation Showing a Transition from Physisorption to Chemisorption, *Science* 366 (6462) (2019) 235–238, eaay3444.
- [43] B. Schuler, W. Liu, A. Tkatchenko, N. Moll, G. Meyer, A. Mistry, D. Fox, L. Gross, Adsorption geometry determination of single molecules by atomic force microscopy, *Phys. Rev. Lett.* 111 (10) (2013) 106103.
- [44] P. Zahl, Y. Zhang, Guide for atomic force microscopy image analysis to discriminate heteroatoms in aromatic molecules, *Energy Fuels* 33 (6) (2019) 4775–4780.
- [45] Y. Zhang, Identify similarities in diverse polycyclic aromatic hydrocarbons of asphaltenes and heavy oils revealed by noncontact atomic force microscopy: aromaticity, bonding, and implications in reactivity, in: P. Rahimi, C. Ovalles, Y. Zhang, J. Adams (Eds.), *Chemistry Solutions to Challenges in the Petroleum Industry*, American Chemical Society 2019.
- [46] N. Pavlicek, A. Mistry, Z. Majzik, N. Moll, G. Meyer, D.J. Fox, L. Gross, Synthesis and characterization of triangulene, *Nat. Nanotechnol.* 12 (4) (2017) 308–311.
- [47] R.A. Greinke, L.S. Singer, Constitution of coexisting phases in mesophase pitch during heat treatment: mechanism of mesophase formation, *Carbon* 26 (5) (1988) 665–670.
- [48] L.S. Singer, I.C. Lewis, D.M. Riffle, D.C. Doetschman, EPR characteristics of separated fractions of mesophase pitches, *J. Phys. Chem.* 91 (9) (1987) 2408–2415.
- [49] B. Alldritt, P. Hapala, N. Oinonen, F. Urtev, O. Krejci, F. Federici Canova, J. Kannala, F. Schulz, P. Liljeroth, A.S. Foster, Automated Structure Discovery in Atomic Force Microscopy, arXiv e-prints, 2019.
- [50] Y. Zhang, Nonalternant aromaticity and partial double bond in petroleum molecules revealed: theoretical understanding of polycyclic aromatic hydrocarbons obtained by non-contact atomic force microscopy, *Energy Fuels* 33 (5) (2018) 3816–3820.
- [51] O.C. Mullins, H. Sabbah, J. Eyssautier, A.E. Pomerantz, L. Barre, A.B. Andrews, Y. Ruiz-Morales, F. Mostowfi, R. McFarlane, L. Goual, R. Lepkowitz, T. Cooper, J. Orbulescu, R.M. Leblanc, J. Edwards, R.N. Zare, Advances in asphaltene science and the Yen-Mullins model, *Energy Fuels* 26 (7) (2012) 3986–4003.
- [52] M.L. Chacón-Patiño, S.M. Rowland, R.P. Rodgers, Advances in asphaltene petroleomics. Part 1: asphaltenes are composed of abundant island and archipelago structural motifs, *Energy Fuels* 31 (12) (2017) 13509–13518.
- [53] F. Alvarez-Ramirez, Y. Ruiz-Morales, Island versus archipelago architecture for asphaltenes: polycyclic aromatic hydrocarbon dimer theoretical studies, *Energy Fuels* 27 (4) (2013) 1791–1808.
- [54] H. Sabbah, A.L. Morrow, A.E. Pomerantz, R.N. Zare, Evidence for island structures as the dominant architecture of asphaltenes, *Energy Fuels* 25 (4) (2011) 1597–1604.